

# FIGRET: Fine-Grained Robustness-Enhanced Traffic Engineering

Ximeng Liu, Shizhen Zhao<sup>\*</sup>, Yong Cui<sup>‡</sup>

Shanghai Jiao Tong University, <sup>‡</sup>Tsinghua University

{liuximeng, shizhenzhao}@sjtu.edu.cn, <sup>‡</sup>cuiyong@tsinghua.edu.cn

## ABSTRACT

Traffic Engineering (TE) is critical for improving network performance and reliability. A key challenge in TE is the management of sudden traffic bursts. Existing TE schemes often struggle to accurately determine the extent of focus required for these surges, thereby facing difficulties in achieving a balance between performance under normal and peak traffic conditions. To address this issue, we introduce FIGRET, a Fine-Grained Robustness-Enhanced TE Scheme. FIGRET offers a novel approach to TE by providing varying levels of robustness enhancements, customized according to the distinct traffic characteristics of various source-destination pairs. By leveraging a sophisticated loss function and advanced deep learning techniques, FIGRET is capable of generating high-quality TE solutions efficiently. Our evaluations of real-world production networks, including Wide Area Networks and data centers, demonstrate that FIGRET significantly outperforms existing TE schemes. Compared to the TE scheme currently deployed in Google’s Jupiter network, FIGRET achieves a 9%-34% reduction in average Maximum Link Utilization and improves solution speed by 35×-1800×. Against DOTE, a state-of-the-art deep learning-based TE method, FIGRET substantially lowers the occurrence of significant congestion events triggered by traffic bursts by 41%-53.9% in topologies characterized by high traffic dynamics.

## 1 INTRODUCTION

With the exponential growth in network traffic, both data centers [5, 6, 11, 14, 16, 37, 43] and Wide Area Networks (WANs) [9, 18, 19, 24–26, 31, 39, 42, 48, 51, 57] are increasingly dependent on Traffic Engineering (TE) for optimizing network flow. TE, typically enabled by a centralized controller in Software-Defined Networking (SDN) [2, 3, 13, 22, 23, 29, 32, 37, 53], periodically solves optimization problems to efficiently route traffic across network paths, translating these solutions into router configurations.

A major challenge in TE is managing sudden traffic bursts. Considering the delays introduced by the central controller in collecting traffic demands, computing new TE solutions,

and updating forwarding rules, TE systems should predefine network configurations based on historical data prior to the arrival of actual traffic flows. Yet, the inherently dynamic and unpredictable nature of real network traffic poses significant forecasting difficulties [45, 50]. Inadequate preparation for these bursts can result in severe network congestion, leading to lengthy delays, high packet loss rates, and diminished network throughput [48]. Thus, enhancing the robustness to respond to unexpected traffic bursts is essential.

Existing TE schemes demonstrate limitations in handling traffic bursts, struggling to determine the appropriate level of intervention for such scenarios. One TE approach to managing traffic bursts is oblivious routing [9], which involves optimizing TE solutions for the worst-case scenario across all traffic demands. While this equips the system to handle bursts, it tends to result in suboptimal performance for typical traffic, which constitutes the majority of traffic over time. Consequently, alternative TE methods [37, 43, 44, 48] do not focus on optimizing for all traffic demands. Instead, they design TE solutions based on historical data while imposing certain constraints to enhance robustness. For example, Google’s hedging mechanism [37] introduces a metric to evaluate the impact of burst traffic on each path, requiring that in solutions, the metric for each path must not surpass a predetermined upper limit. Since optimization occurs based on historical traffic matrices, the impact on average performance is less significant compared to oblivious routing. However, depending solely on a single constraint for optimization often fails to achieve a satisfactory balance in TE performance across regular and bursty traffic conditions.

The limitations observed in previous methods can be attributed to their excessively broad approach to enhancing robustness. These methods adopt a perspective grounded in a traffic matrix that encompasses flows from all source-destination pairs across the entire network. In doing so, they treat the traffic of each pair indiscriminately and uniformly. However, in practice, network traffic exhibits significant variations among different source-destination pairs. While some pairs may encounter traffic bursts, others may maintain remarkable stability. For consistently stable traffic, prioritizing

<sup>\*</sup>Shizhen Zhao is the corresponding author.

robustness becomes unnecessary and may even result in performance compromises during regular traffic conditions.

Building upon this observation, we design FIGRET (Fine-Grained Robustness-Enhanced Traffic Engineering). FIGRET’s *key insight* lies in a fine-grained customized robustness enhancement strategy, tailored for individual source-destination pairs based on their traffic characteristics. It applies relaxed robustness requirements to source-destination pairs with stable traffic and enforces stricter requirements for those prone to bursts. In the initial phase, we employ a metric called path sensitivity [43] to measure the impact of burst traffic on network paths, thus enabling robustness enhancement through the application of path sensitivity constraints. To achieve fine-grained robustness and ensure a satisfactory balance in TE performance across both normal and bursty traffic conditions, we customize the path sensitivity constraints according to the network topology and the traffic characteristics of the source-destination pairs they connect, while also considering this path sensitivity constraint when optimizing based on historical data. To accomplish this, FIGRET leverages a deep neural network equipped with a well-designed loss function, which includes two components: one for evaluating performance under normal traffic conditions and another for assessing robustness. Moreover, we employ an efficient network architecture for FIGRET.

We conducted a comprehensive evaluation of FIGRET. This evaluation utilized publicly available WAN datasets [46], as well as Data Center PoD-level and ToR-level topologies and traffic data [7, 40]. The data encompassed topologies ranging from dozens to hundreds of nodes, with the corresponding traffic data exhibiting various characteristics, including stable, composite, and bursty profiles. Through our evaluation, we found that FIGRET consistently delivers high-quality TE solutions across a variety of topologies. Compared to the TE system currently in production by Google’s Jupiter [37], FIGRET achieved an average Max Link Utilization (MLU) reduction of 9%-34% across different topologies and improved solution speed by 35×-1800×. In comparison with the state-of-the-art Deep Learning-based TE system DOTE [36], specifically designed for MLU optimization, FIGRET achieved notable improvements in two topologies with bursty traffic data. It reduced the average Max Link MLU by 4.5% and 5.3% while simultaneously decreasing the number of significant congestion incidents caused by traffic bursts by 41% and 53.9%. Meanwhile, in topologies with stable traffic data, FIGRET performed at least as well as DOTE, despite the additional consideration of robustness. Additionally, we provided interpretability for the workings of FIGRET.

This work does not raise any ethical concerns.

## 2 MOTIVATION AND KEY INSIGHTS

To motivate our fine-grained robustness enhancement method, we first demonstrate that different source-destination pairs within a network exhibit distinct traffic characteristics (§2.1). Subsequently, we illustrate the necessity for robustness in TE correlates with traffic characteristics. By tailoring robustness requirements according to the traffic characteristics, TE becomes more effective than treating all source-destination pairs as equal (§2.2).

### 2.1 Diversity in traffic characteristics

To demonstrate the diverse traffic characteristics under different source-destination pairs (SD pairs), we provide an analysis of traffic characteristics across SD pairs in various production networks. This includes the WAN network GEANT [46], as well as the Facebook data center network [40] at both the PoD-level and ToR-level. Details on the public data used are provided in §5. For each SD pair, we calculate the variance as a measure of the dynamic changes in traffic. The results of our analysis are displayed in Figure 1, which shows the *variance* of traffic demand for different SD pairs across the three types of network traffic. The greater the variance for a SD pair, the more unstable that SD pair is.

The results in Figure 1 indicate that, regardless of the topology type, there are distinct traffic characteristics for different SD pairs. It is inappropriate to consider all traffic within these SD pairs as uniform, as this approach inevitably leads to a *trade-off* in TE. If TE treats all SD pairs as non-bursty traffic, it sacrifices the ability of TE to handle bursty traffic effectively. On the other hand, treating all SD pairs as bursty traffic results in suboptimal performance under non-bursty conditions. So, we seek a method that can differently consider SD pairs with varying traffic characteristics.

### 2.2 Dig deep into the trade-off

**Trade-off dilemma in TE.** In TE, there is a challenging trade-off between the ability to handle burst traffic and the performance in non-burst scenarios. To illustrate the trade-off dilemma in TE, we present an illustrative example in Figure 2. In this network, there are three traffic demands:  $A \rightarrow B$ ,  $A \rightarrow C$ ,  $B \rightarrow C$ . In the typical situation, the traffic demand for all three is 1. However, in three different burst situations, the traffic demand for  $A \rightarrow B$ ,  $A \rightarrow C$ ,  $B \rightarrow C$  increases to 4, respectively.

TE scheme 1 considers all traffic as non-bursty and only optimizes for the typical situation. To minimize congestion in non-bursty scenarios, TE scheme 1 directs all traffic along the shortest paths. In the typical situation, its Max Link Utilization (MLU) is  $\max\{\frac{1}{2}, \frac{1}{2}, \frac{1}{2}\} = 0.5$ . When any burst situation occurs, the MLU is  $\max\{\frac{4}{2}, \frac{1}{2}, \frac{1}{2}\} = 2$ .

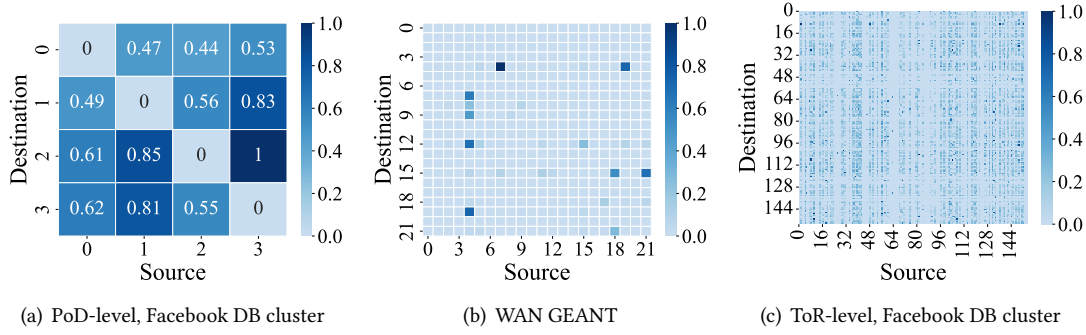


**Figure 1: The variance of traffic demand by source and destination (The value of variance has been normalized). The larger the variance, the more likely it is that the traffic demand for that source-destination pair will experience a burst. Regardless of which network in 1(a), 1(b), or 1(c), the traffic demands of different source-destination pairs exhibit different traffic characteristics.**

TE scheme 2 considers all traffic as bursty traffic and aims to enhance robustness in response to the three burst situations by splitting traffic across different paths. When dealing with the typical situation, the MLU of TE scheme 2 is  $\max\{\frac{1 \times 0.5 + 1 \times 0.5 + 1 \times 0.5}{2}, \frac{1 \times 0.5 + 1 \times 0.5 + 1 \times 0.5}{2}, \frac{1 \times 0.5 + 1 \times 0.5 + 1 \times 0.5}{2}\} = 0.75$ , while dealing with the three burst situations, its MLU is  $\max\{\frac{4 \times 0.5 + 1 \times 0.5 + 1 \times 0.5}{2}, \frac{4 \times 0.5 + 1 \times 0.5 + 1 \times 0.5}{2}, \frac{4 \times 0.5 + 1 \times 0.5 + 1 \times 0.5}{2}\} = 1.5$ . That is, TE scheme 2 exhibits better robustness in handling traffic bursts compared to TE scheme 1, but with a decrease in typical performance.

Overall, this one-size-fits-all approach either leads to a network lacking the capacity to handle bursts or enhances the capability to manage bursts but at the cost of compromised performance in non-burst situations. This trade-off presents a dilemma for TE to address.

**A key insight in balancing typical performance and robustness.** We find that a more effective approach is to differentiate treatment based on the unique characteristics of each SD pair. Figure 2(e) illustrates this point. TE scheme 3 specifically addresses the bursts between  $B \rightarrow C$ , selecting two paths for serving the traffic from B to C. Conversely, for  $A \rightarrow B$  and  $A \rightarrow C$ , it opts for direct paths. In TE scheme 3, the MLU is  $\max\{\frac{1 \times 0.375 + 1}{2}, \frac{1 \times 0.375 + 1}{2}, \frac{1 \times 0.625}{2}\} = 0.6875$  under the typical situation. And when dealing with either traffic burst situation 1 or 2, the MLU is  $\max\{\frac{1 \times 0.375 + 4}{2}, \frac{1 \times 0.375 + 1}{2}, \frac{1 \times 0.625}{2}\} = 2.1875$ , while dealing with the traffic burst situation 3, the MLU is  $\max\{\frac{4 \times 0.375 + 1}{2}, \frac{4 \times 0.375 + 1}{2}, \frac{4 \times 0.625}{2}\} = 1.25$ . It can be observed that, although TE scheme 3 is not as robust as TE scheme 2 in handling traffic burst situation 1/2, it performs better than TE scheme 2 in both typical situations and traffic burst situation 3. If the traffic demand from A to B and A to C never experiences traffic bursts, then TE scheme 3 would be a better solution compared to TE scheme 2. That is, if a traffic

demand remains consistently stable, then the robustness of the paths serving that traffic demand does not need to be a concern (similar to how TE scheme 3 does not consider the robustness of path  $A \rightarrow B$  and path  $A \rightarrow C$ ).

Based on insights from Figure 1 and Figure 2, it is evident that enhancing robustness to manage unexpected traffic bursts is necessary. However, uniformly increasing the robustness across all paths may lead to a compromise in average performance. A more nuanced strategy would be to adjust the robustness of paths based on the traffic characteristics of the traffic demands they serve. This strategy, which refines the robustness enhancement at a finer granularity compared to previous TE methods, enables a better balance between typical performance and robustness in TE.

### 3 TE MODEL

**Notations & Definitions.** We introduce recurring mathematical notations and definitions of TE. All notations used in this paper are also tabulated in Table 5 for ease of reference.

- **Network.** We represent the network topology as a graph  $G = (V, E, c)$ , where  $V$  and  $E$  are the vertex and edge sets, respectively, and  $c : E \rightarrow \mathbb{R}^+$  assigns capacities to edges.
- **Traffic demands.** A Demand matrix (DM)  $D$  is a  $|V| \times |V|$  matrix whose  $(i, j)$ 'th entry  $D_{ij}$  specifies the traffic demand between source  $i$  and destination  $j$ .
- **Network paths.** Each source vertex  $s$  communicates with each destination vertex  $d$  via a set of network paths  $P_{sd}$ . We can also say that  $P_{sd}$  serves the SD pair.
- **Path capacity.** The capacity of a path  $p$  is denoted by  $C_p$ . It is the minimum capacity across the edges comprising the path [37].
- **TE configuration.** A TE configuration  $\mathcal{R}$  specifies for each source vertex  $s$  and destination vertex  $d$  how the  $D_{sd}$  traffic from  $s$  to  $d$  is split across the paths in  $P_{sd}$ . A TE

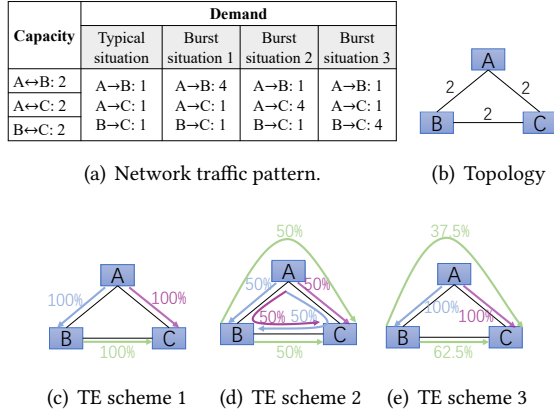


**Figure 2: A simple example comparing three TE schemes. TE scheme 1 has the optimal MLU in the typical situation. When traffic burst situations 1/2/3 are all possible, TE scheme 2 exhibits the best resilience against bursts. However, if only traffic burst situation 3 is likely to occur, TE scheme 3 outperforms TE scheme 2.**

configuration specifies for each path  $p \in P_{sd}$  a split ratio  $r_p$ , where  $r_p$  is the fraction of the traffic demand from  $s$  to  $d$  forwarded along path  $p$  ( $\sum_{p \in P_{sd}} r_p = 1$ ).

- **TE objective.** Our TE objective is to minimize the max link utilization (MLU), which is a classical TE objective [10, 11, 17, 37, 47]. Google found MLU to be a reasonable proxy metric for throughput as well as for resilience against traffic pattern variation. They found high MLU indicates many links are in danger of overloading, causing packet losses, increasing flow-completion time, and reducing throughput [37].

Given a demand matrix  $D$  and TE configuration  $\mathcal{R}$ , the traffic flow traversing edge  $e$  is  $f_e = \sum_{s,d \in V, p \in P_{sd}, e \in p} D_{sd} \cdot r_p$ , then the MLU induced by  $D$  and  $\mathcal{R}$  is  $\text{MLU} = \max_{e \in E} \frac{f_e}{c(e)}$ , which we denote as  $M(\mathcal{R}, D)$ .

**TE under traffic uncertainty.** At epoch  $t$ , the decision maker in TE must output a network configuration  $\mathcal{R}_t(D_1, \dots, D_{t-1})$  based on historical data  $\{D_1, \dots, D_{t-1}\}$  before the arrival of  $D_t$ . The goal is to ensure that this configuration consistently yields low link over-utilization for the upcoming traffic  $D_t$ .

$$\underset{\mathcal{R}_t(D_1, \dots, D_{t-1})}{\text{minimize}} \quad M(\mathcal{R}_t(D_1, \dots, D_{t-1}), D_t) \quad (1)$$

When configuring  $\mathcal{R}_t$  based on historical data  $\{D_1, \dots, D_{t-1}\}$  before the arrival of  $D_t$ , it is critical to consider both anticipated and unanticipated traffic. Firstly, an anticipated traffic demand  $D_t^{\text{expect}}$  is deduced from historical traffic data. This

expected demand may be explicitly obtained through predictive modeling or implicitly represent the insights gleaned from past data trends. Concurrently, acknowledging the inevitable discrepancies between anticipated and actual traffic due to mis-prediction, it is crucial to incorporate the impact of such mismatches when calculating the TE configuration.

## 4 FIGRET DESIGN

In this section, we present the design of FIGRET. In §4.1, we introduce how FIGRET addresses traffic bursts while solving TE solutions based on historical traffic. Subsequently, §4.2 discusses the transformation of problem-solving into the design of loss functions using deep learning. The design of the loss function and the network architecture are then detailed in §4.3 and §4.4, respectively. Finally, §4.5 also covers how FIGRET handles link failures.

### 4.1 Design for managing traffic bursts

As outlined in §3, it is not adequate for TE to rely solely on  $D^{\text{expect}}$  obtained from historical data. To augment robustness, the impact of traffic bursts must be considered.

**By defining a set to account for traffic bursts.** A prevalent method involves defining the mismatch as a set  $\Delta$ . During the optimization process, the sum of a specific mismatch  $\delta$  from  $\Delta$  and  $D^{\text{expect}}$  is used as an estimate for the actual traffic, denoted as  $\hat{D}_t = \delta + D^{\text{expect}}$ . TE configurations are then determined based on  $\hat{D}_t$ , i.e.,

$$\begin{aligned} & \underset{\mathcal{R}_t}{\text{minimize}} && \max_{\hat{D}_t \in \hat{\mathcal{D}}} M(\mathcal{R}_t, \hat{D}_t) \\ & \text{subject to} && \hat{\mathcal{D}} = \{\hat{D}_t | \hat{D}_t = \delta + D^{\text{expect}}, \delta \in \Delta\} \end{aligned} \quad (2)$$

*Drawback:* Adjusting the size of the set  $\Delta$  allows for the modulation of the algorithm's emphasis on traffic bursts. However, defining this set accurately is quite challenging. A larger set size implies that TE takes into account a greater traffic variability, which, while potentially increasing the algorithm's robustness, may diminish its focus on  $D^{\text{expect}}$ . Conversely, a smaller set size means fewer traffic variable scenarios are considered, potentially compromising robustness. Therefore, this approach is not considered in our design.

**By imposing constraints to account for traffic bursts.** When considering both  $D^{\text{expect}}$  and  $\Delta$ , the utilization of each edge can be expressed as:  $\sum_{s,d \in V, p \in P_{sd}, e \in p} (D_{sd}^{\text{expect}} + \delta_{sd}) \cdot r_p / c(e)$ . Consequently, the actual impact of  $\delta_{sd}$  on each edge can be represented by its coefficient. To mitigate this impact, it is essentially about ensuring that this coefficient is less than a certain constraint. The degree of robustness can be controlled by adjusting the stringency of this constraint.

As discussed in §2, we aim to impose varying degrees of robustness on different paths based on the traffic characteristics of the SD pairs. Therefore, this constraint should be a

function related to the SD pairs, defined as  $\mathcal{F} : (s, d) \rightarrow \mathbb{R}^+$ .

$$\forall s, d \in V, \forall p \in P_{sd}, \forall e \in P \quad \frac{r_p}{c(e)} \leq \mathcal{F}((s, d)) \quad (3)$$

Considering the definitions of path capacity  $C_p$ , as expressed by  $C_p = \min_{e \in p} c(e)$ , it follows that Equation 3 is equivalent to Equation 4.

$$\forall s, d \in V, \forall p \in P_{st} \quad \frac{r_p}{C_p} \leq \mathcal{F}((s, d)) \quad (4)$$

As indicated in Equation 4, ensuring that the ratio  $\frac{r_p}{C_p}$  falls within certain constraints guarantees the robustness of network configurations against burst traffic. Therefore  $\frac{r_p}{C_p}$  can be used as a metric to represent the degree of robustness in the network configuration. So we define path sensitivity  $\mathcal{S}_p$  for path  $p$  as

$$\mathcal{S}_p = \frac{r_p}{C_p}$$

By taking into account the metric of path sensitivity when specifying TE configurations and ensuring it meet certain constraints, TE can be aided in minimizing the impact of  $D^{\text{burst}}$  on network performance. Therefore, our solution can be expressed as Equation 5.

minimize $M(\mathcal{R}_t, D_t^{\text{expect}})$ subject to $\mathcal{S}_p \leq \mathcal{F}((s, d)), \forall s, d \in V, \forall p \in P_{sd}$	(5)
---	-----

**Remark.** In Equation 5, both  $D_t^{\text{expect}}$  and  $\mathcal{F}$  are determined based on historical traffic data  $\{D_1, \dots, D_{t-1}\}$ . Selecting an appropriate  $D_t^{\text{expect}}$  and  $\mathcal{F}$  for a specific network topology and traffic pattern is not trivial. Existing methods have not finely discriminated between different SD pairs. For example:

- Traditional methods based on direct optimization of MLU after prediction, as well as those based on deep learning [36, 47], set  $\mathcal{F}((s, t)) \equiv +\infty, \forall s, t \in V$ . They assume that the real flow can be entirely represented by  $D^{\text{expect}}$ . However, due to the inherent dynamic nature of traffic demands, mismatches are inevitable.
- Desensitization-based TE schemes [37] set  $\mathcal{F}((s, d)) \equiv \text{const}, \forall s, d \in V$ . A single constant value makes it challenging to perfectly balance burst resistance and average performance. Another approach [44] sets  $\mathcal{F}((s, d))$  as an objective, aiming to minimize the maximum  $\mathcal{F}((s, d))$  among all SD pairs. However, it also does not account for differences among SD pairs. Even if a stable SD pair has a larger  $\mathcal{F}((s, d))$ , it would not impact robustness.

## 4.2 FIGRET framework

In this section, we explain the overall framework of FIGRET for solving Equation 5. To solve Equation 5, we first consider the following: both  $D_t^{\text{expect}}$  and  $\mathcal{F}$  are determined based

on historical traffic data  $\{D_1, \dots, D_{t-1}\}$ . If the mapping relationship between  $\{D_1, \dots, D_{t-1}\}$  and both  $D_t^{\text{expect}}$  and  $\mathcal{F}$  is already known, then Equation 5 can be directly solved. Therefore, the framework for solving Equation 5 is divided into two types based on whether an explicit  $D_t^{\text{expect}}$  and  $\mathcal{F}$  are pre-determined.

The first approach involves, initially, attempting to explicitly solve for  $D_t^{\text{expect}}$  and  $\mathcal{F}$ , followed by employing a linear programming-based algorithm to solve the Equation 5. However, this method encounters two main issues. First, there is a mismatch [36] between predicting  $D_t^{\text{expect}}$  accurately and the ultimate goal of TE, which is to minimize MLU. This mismatch arises due to the influence of network topology and edge capacities; accurately predicting certain flows is more crucial than others. For instance, accurately predicting traffic for SD pairs with paths of high capacity is less critical. But the objective of accurate prediction (usually employing mean-squared-error, etc., as the loss) does not account for this. An example is illustrated in Figure 16. As for  $\mathcal{F}$ , it is even more challenging to define a specific approach to find an optimal  $\mathcal{F}$ . Second, using linear programming introduces substantial computational delays, and the algorithm's scalability to network topology is not guaranteed. Therefore, the approach of first solving for  $D_t^{\text{expect}}$  and  $\mathcal{F}$  before solving the problem is not ideal.

An alternative approach eschews the explicit computation of  $D_t^{\text{expect}}$  and  $\mathcal{F}$ . Instead, it directly establishes an end-to-end relationship between historical traffic data  $\{D_1, \dots, D_{t-1}\}$  and a TE configuration  $R_t$  that aims to minimize MLU and assures robustness. The fundamental effectiveness of this method lies in its intrinsic capability to implicitly weigh the importance of different SD pairs based on network topology and capacity. This effectively mitigates the previously observed mismatch between obtaining  $D_t^{\text{expect}}$  and  $\mathcal{F}$ , and the ultimate goal of minimizing MLU. Based on the above considerations, we also adopt this approach in FIGRET.

**Leveraging Deep Learning** Although we recognize the need to establish an end-to-end relationship between historical traffic data  $\{D_1, \dots, D_{t-1}\}$  and a TE configuration  $R_t$  that minimizes MLU and assures robustness, the complexity of network topologies and real-world traffic patterns defy straightforward mathematical characterization. In response, FIGRET adopts a deep neural network (DNN) approach, effectively sidestepping the complexities of directly solving Equation 5 by reframing the challenge into a well-designed loss function that captures the essence of the optimization problem. The powerful learning capabilities of DNNs are leveraged to effectively approximate the solution to Equation 5, accommodating the dynamic and uncertain nature of network traffic and topology.

### 4.3 Design loss function of FIGRET

In FIGRET, a Deep Neural Network (DNN) is employed to establish a mapping between historical traffic data,  $\{D_1, \dots, D_{t-1}\}$ , and TE configurations. The input to FIGRET comprises historical traffic data, while its output is a TE configuration. To maintain a consistent input size for the DNN and prevent an overload of traffic data when  $t$  is large, a temporal window  $H$  is typically chosen [36, 47]. This leads to the use of traffic data within this window,  $\{D_{t-H}, \dots, D_{t-1}\}$ , as the input. During training, FIGRET receives  $\{D_{t-H}, \dots, D_{t-1}\}$ , and subsequently outputs a TE Configuration  $R_t$ . We denote this output as  $R_t = \pi_\theta(D_{t-H}, \dots, D_{t-1})$ , where  $\pi$  represents the mapping function from DNN inputs to outputs, and  $\theta$  denotes the DNN's link weights. The revealed  $D_t$  allows for the calculation of the loss for this  $R_t$  through the loss function  $\mathcal{L}(R_t, D_t)$ , after which a gradient descent optimizer updates the parameters  $\theta$ . Thus, to enable FIGRET to approximate the solution to Equation 5, a *well-designed loss function* is essential. This function must capture the essence of the optimization problem, guiding the neural network towards effective and efficient solutions.

**Loss function design.** The design of our loss function is intrinsically aligned with the Lagrangian relaxation of Equation 5, as delineated in Equation 6.

$$\begin{aligned} & \underset{\mathcal{R}_t, \lambda}{\text{minimize}} && L(\mathcal{R}_t, \lambda) = M(\mathcal{R}_t, D_t^{\text{expect}}) \\ & + \sum_{s,d \in V} \sum_{p \in P_{sd}} \lambda_{sd} (\mathcal{S}_p - \mathcal{F}((s, d))) \\ & \text{subject to} && \lambda_{sd} \geq 0, \quad \forall s, d \in V, \forall p \in P_{sd} \end{aligned} \quad (6)$$

This relaxation framework guides us in structuring a loss function that encompasses two components. The first component corresponds to minimizing max link utilization.

$$\mathcal{L}_1 = M(R_t, D_t), \quad (7)$$

With the first loss function in place, upon completion of training, FIGRET *implicitly* learns a probability distribution  $P(D_t^{\text{expect}} | D_{t-1}, \dots, D_{t-H})$ . It can then output an  $R_t$  that optimizes  $\mathbb{E}_{D_t^{\text{expect}}} [M(\mathcal{R}_t, D_t^{\text{expect}})]$  with respect to  $P(D_t^{\text{expect}} | D_{t-1}, \dots, D_{t-H})$  ( $D_t^{\text{expect}}$  can be multiple). This illustrates that optimizing MLU directly, rather than focusing on the accuracy of  $P(D_t | D_{t-1}, \dots, D_{t-H})$ , essentially employs network topology and capacity information to weight  $P(D_t | D_{t-1}, \dots, D_{t-H})$ . This approach effectively resolves the mismatch between prediction accuracy and the objective of minimizing MLU.

The second component of the loss function reflects the constraints imposed by path sensitivities. We use  $\sigma_{D_{sd}, [1-T]}^2$  to denote the variance of traffic demands  $D_{sd}$  from source  $s$  to destination  $d$  within the time range from 1 to  $T$ . We denote

$\mathcal{S}_{sd}^{\max}$  as the maximum path sensitivity among all paths serving from source  $s$  to destination  $d$  in the configuration  $\mathcal{R}_t$ . Based on this, we can express  $\mathcal{L}_2$  as Equation 8.

$$\mathcal{L}_2 = \sum_{\forall s, d \in V} \sigma_{D_{sd}, [1-T]}^2 \times \mathcal{S}_{sd}^{\max}, \quad (8)$$

The rationale behind the formulation of  $\mathcal{L}_2$  is rooted in the differential treatment of path sensitivities across various source-destination (SD) pairs, guided by the constraints  $\mathcal{F}((s, d))$ . In essence, for SD pairs exhibiting stable traffic patterns, denoted as  $(s, d)_{\text{stable}}$ , the model enforces less stringent path sensitivity constraints. Conversely, for SD pairs characterized by bursty traffic dynamics, labeled as  $(s, d)_{\text{bursty}}$ , the model imposes stricter path sensitivity restrictions. This distinction is encapsulated in the relationship  $\mathcal{F}((s, d)_{\text{stable}}) > \mathcal{F}((s, d)_{\text{bursty}})$ . In other words, assuming in a given scenario  $\mathcal{S}_{sd_{\text{bursty}}}^{\max} = \mathcal{S}_{sd_{\text{stable}}}^{\max}$ , the bursty traffic SD pair might incur a greater penalty. To ensure  $\mathcal{L}_2$  is designed to meet this criterion, we calculate the variance of traffic demand  $\sigma_{D_{sd}, [1-T]}^2$  for each SD pair from time 1 to  $T$ , representing the degree of variation in the flow. This provides a quantitative measure of traffic fluctuation for the network. Subsequently, we weight these variances against the maximum path sensitivity  $\mathcal{S}_{sd}^{\max}$  of paths serving the corresponding SD pair. This approach imposes stricter sensitivity penalties on flows with higher variance and lighter penalties on those with lower variance. Such a weighted method effectively differentiates between various traffic characteristics, making corresponding adjustments to the impact on network performance.

When training the neural network, we consider both the loss term MLU  $\mathcal{L}_1$  and the plenty term  $\mathcal{L}_2$ . This comprehensive consideration aims to guide the network in learning how to adjust path sensitivity constraints for different SD pairs while maintaining MLU optimization. By this method, we ensure that the network not only meets the MLU optimization objectives but also enhances the burst resistance of different SD pairs in a fine-grained manner.

### 4.4 Design DNN structure of FIGRET

The structures primarily used in TE are as follows: Graph Neural Network (GNN) [12, 51], Convolutional Neural Network (CNN) [47], and Fully Connected Network (FCN) [36]. In this section, we briefly explain why we chose FCN over GNN and CNN, with more detail placed in Appendix D.

**Network topology handling: no need for GNN.** In TE problems, acquiring and utilizing network topology information is crucial for constructing the mapping between TE configurations and MLU. The network topology  $G(V, E, c)$ , as a graph structure, seems naturally suited for processing



with GNN. However, as Function 1 shows, this mapping relationship can be achieved through simple matrix operations, which can be fully handled by FCN. GNN involves processing based on adjacency matrices and node features, which can lead to redundant computations and higher computational complexity, potentially consuming significant memory [49, 52, 55]. Considering these factors, using FCN as a more efficient alternative seems a more reasonable choice.

**CNN vs. FCN: The inappropriateness of CNN.** CNN can effectively extract local information in data such as images through convolutional operations. However, in the historical traffic demand data used as input for TE, there is no obvious local information. The traffic sharing a common edge can be spatially close or distant, not necessarily confined to a local area. A detailed example is provided in Figure 11. Therefore, we opted not to use CNN, but rather FNN.

#### 4.5 Coping with link failures

Tunneling protocols are instrumental in identifying paths with failed nodes or links. A traditional approach to addressing link failures in TE involves rerouting traffic around failed paths by allowing traffic sources to proportionally redistribute traffic among their remaining paths [22, 23, 36, 42].

- In cases where the remaining paths have predefined allocation ratios, the traffic demand from a failed path is proportionally redistributed based on these ratios. Consider a scenario with three paths having allocation ratios of (0.5, 0.3, 0.2). If the first path experiences a failure, the adjusted distribution ratios for the remaining paths would be recalculated to (0, 0.6, 0.4).
- Conversely, if the remaining paths do not have predefined allocation ratios, the traffic demand from the failed path is equally distributed among them. For instance, in a situation with three paths at ratios (1, 0, 0), and the first path becomes inoperable, the redistributed traffic is allocated evenly, resulting in new ratios of (0, 0.5, 0.5).

We integrate this approach into FIGRET, evaluate its effectiveness, and demonstrate that it achieves high resiliency to failures in §5.3. Notably, handling link failures in FIGRET does not necessitate retraining.

## 5 EVALUATION

In this section, we evaluate FIGRET. In §5.1, we first describe our evaluation methodology and analyze the types of traffic used in the evaluation to demonstrate that our experiments cover a wide variety of traffic scenarios. Subsequently, in §5.2, we compare FIGRET with state-of-the-art TE schemes, focusing on TE quality, solution times, and precomputation times. Then, the effectiveness of FIGRET in handling link failures and adapting to drifts in traffic patterns is evaluated in §5.3

and §5.4, respectively. Finally, in §5.5, we showcase the adaptive robustness enhancement capabilities of FIGRET, thereby providing an interpretation of FIGRET’s performance.

### 5.1 Methodology

**Topologies.** We consider three WAN topologies, including the pan-European research network, GEANT [46], as well as two topologies from the Internet Topology Zoo [28], namely UsCarrier and Kdl. We also examine various topologies within the data center (DC). This includes the pFabric [7], which utilizes a leaf-spine topology, featuring nine Top-of-Rack (TOR) switches. Each ToR switch in the pFabric architecture is connected to all spine switches, forming a network that is logically equivalent to a fully-connected topology. Additionally, we consider two Facebook DC clusters [40]: the Facebook DB cluster and the Facebook WEB cluster. The Facebook DB cluster comprises MySQL servers that store user data and handle SQL queries, whereas the Facebook WEB cluster is responsible for serving web traffic. For each cluster, we contemplated two types of topologies: the Top-of-Rack (ToR) level and the Point of Delivery (PoD) level. For the PoD level topology, we consider the fat-tree architecture [4], whereas for the ToR level topology, the Jellyfish architecture [41] is taken into account. Their numbers of nodes and edges are summarized in Table 1. For each topology, we employ Yen’s algorithm to precompute three shortest paths between every pair of nodes as the candidate paths for flow allocation [1, 34].

	#Type	#Nodes	#Edges
GEANT	WAN	23	74
UsCarrier	WAN	158	378
Cogentco	WAN	197	486
pFabric	ToR-level DC	9	72
Facebook DB	PoD-level DC	4	12
	ToR-level DC	155	7194
Facebook WEB	PoD-level DC	8	56
	ToR-level DC	324	31520

**Table 1: Network topologies in our evaluation.**

**Traffic data.** For the GEANT topology, there are publicly available traffic matrix traces, which consist of data aggregated every 15 minutes over four months [46]. In the context of pFabric topology, the pFabric trace is characterized by a Poisson arrival process. When a flow arrives, the source and destination nodes are chosen uniformly at random from a set of 9 different ToR switches. The size of each flow is determined randomly, adhering to the distribution outlined in the "web search workload" scenario as described in [7]. In the case of the Facebook topology, there is a public trace of one day’s traffic [40]. For the PoD-level topology, we aggregate traces into 1-second averaged snapshots of the inter-Pod

traffic matrix, while for the ToR-level topology, aggregation is performed into 10-second averaged snapshots of the inter-ToR traffic matrix. The longer aggregation time for ToR-level topologies is attributed to their larger scale, which involves more nodes and a more complex network structure, resulting in greater computational and storage demands for TE. For the UsCarrier and Kdl topologies from Topology Zoo, where no public traffic traces are available, we employ a gravity model [9, 38] to generate synthetic traffic.

**Traffic characteristics.** Our data includes different types of topologies and their corresponding traffic, each with distinct traffic characteristics. By comparing the similarity of the currently-seen TM with historical TMs, we observe whether the traffic is relatively stable and predictable. To verify this property, for every currently-seen TM, we consider a window of historical TMs, find the TMs that most closely resemble this currently-seen TM, and calculate the cosine similarity between the two. Figure 3 shows the distribution of the results. Each candlestick displays the distribution of cosine similarities for different traffics, with the box range extending from the 25th to the 75th percentile. The closer the distribution of a traffic’s cosine similarity is to 1, the more similar it is to past traffic, indicating greater stability. Conversely, a cosine similarity closer to 0 suggests that the traffic is more erratic.

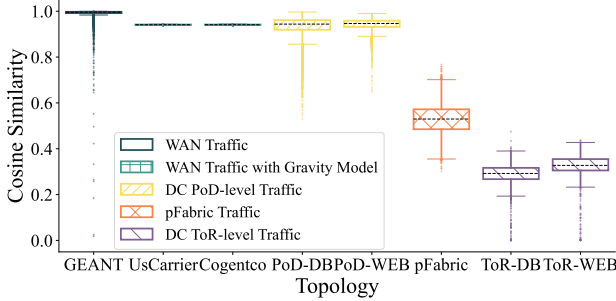


**Figure 3: Cosine similarity analysis using a window of 12 historical TMs vs. the currently-seen TM.**

We can identify the following characteristics:

- The degree of burstiness in traffic increases progressively from WAN traffic to DC POD-level traffic, to DC ToR-level traffic. This may be related to the aggregation of traffic; POD-level traffic aggregates ToR-level traffic, and the WAN connects different data centers, making the aggregation effect more pronounced. The aggregation of multiple traffic streams can cause the bursty variations of different traffic to ‘neutralize’ each other, hence the more aggregation there is, the more stable the traffic becomes.
- Even though WAN traffic is generally stable, there are some anomalies in the cosine similarity distribution of publicly

available WAN Traffic, indicating that WAN traffic can sometimes experience sudden bursts.

- Although the WAN traffic generated by the gravity model closely resembles real WAN traffic, the cosine similarity distribution of the traffic generated by the gravity model does not contain anomalies, indicating the traffic is very stable, making TE solutions relatively straightforward.

In summary, the traffic data we have chosen covers a range of traffic characteristics, including stable WAN traffic, highly bursty DC ToR-level traffic, and moderately variable PoD-level traffic. This allows for a thorough testing of the TE solver’s performance in various scenarios.

**Baseline.** To evaluate the effectiveness of FIGRET improvements relative to other TE schemes, we select the following TE schemes for evaluation: (1) **Omniscient TE**: This scheme represents an optimization with perfect knowledge of future demands, providing a benchmark for the most efficient performance achievable in all TE schemes. (2) **Desensitization-based TE**: This is the TE scheme used by Google in Jupiter [37] and [43]. This scheme constructs an anticipated matrix composed of the peak values for each source-destination pair within a time window. The optimization of the TE objective is then carried out under the constraint that the sensitivity of each path remains below a certain threshold. (3) **Demand-oblivious TE** [9]: This scheme focuses on optimizing the worst-case performance across all possible traffic demands. (4) **Demand-prediction-based TE** [1, 22, 23]: This method involves predicting the next incoming traffic demand and configuring accordingly, *without* considering the mis-predictions that may arise from the traffic uncertainty. (5) **COPE** [48]: This scheme enhances demand-oblivious TE by also optimizing over a set of predicted traffic demands. It optimizes MLU across a set of DMs spanned by previously observed DMs while retaining a worst-case performance guarantee. (6) **Deep Learning-based TE (DOTE)** [36]: DOTE employs a DNN to directly output the TE configuration based on the traffic demand observed within a given time window. (7) **TEAL** [51]: TEAL employs a combination of GNN and Reinforcement Learning (RL) to process a given traffic demand, subsequently outputting a network configuration tailored for this demand. In our experiments, due to the absence of prior knowledge about future traffic, we adopt the network configuration generated based on the traffic demand of the preceding time snap.

**Infrastructure and software.** Our experiments are carried out on an Intel(R) Xeon(R) Silver 4110 CPU, equipped with 128GB of memory. Furthermore, Nvidia-Tesla P100 GPUs are accessible for all schemes, but only FIGRET, DOTE, and TEAL can utilize them. We implement FIGRET using PyTorch [35]. For TE schemes that necessitate solving optimization problems, Gurobi (version 9.5.2) [20] is employed.



## 5.2 Comparing with other TE schemes

**TE quality.** Figure 4 compares the quality of TE solutions between FIGRET and other TE schemes. The y-axis value represents the MLU normalized by that of the Omniscient TE. We note the findings:

- **Desensitization-based TE.** Across all topologies, the performance of Desensitization-based TE in terms of both typical MLU (represented by the box) and the worst-case MLU (indicated by the top of the upper dashed line) is not satisfactory. This is due to the fact that Desensitization-based TE imposes unnecessary path sensitivity constraints on non-bursty traffic while providing insufficient path sensitivity constraints for bursty traffic. We will more clearly illustrate this using Figure 6 in §5.5.
- **Demand-prediction-based TE.** Demand-prediction-based Traffic TE methods primarily excel in environments with stable traffic demands. However, their effectiveness significantly diminishes in sudden or unexpected traffic bursts. The performance of these methods is highly dependent on the accuracy of traffic demand predictions.
- **Demand-oblivious TE & COPE.** Due to the extensive computation time and memory requirements of Demand-oblivious TE and COPE, we are only able to use a few smaller-scale topologies. The two methods for handling mis-prediction are essentially the use of a set-based approach as introduced in §4.1. It is evident that selecting a set not only increases computational complexity but also makes it difficult to achieve a good balance between typical performance and robustness to traffic bursts.
- **DOTe.** DOTe, the best-performing algorithm in existing TE [36], leverages deep learning to link historical traffic data with imminent network configurations, achieving outstanding typical performance. DOTe implicitly learns to achieve the lowest expected MLU with  $D^{\text{expect}}$ , reaching the optimal average performance among existing methods. However, its drawback lies in handling burst situations. For example, in the GEANT data, as shown in Figure 3, while most of the data points have high cosine similarity, close to 1, there are some outliers where the traffic’s cosine similarity with past window traffic is very low, representing exceptional cases. This leads to DOTe’s MLU performance on GEANT data being close to that of Omniscient in most situations but with some high values. As illustrated in Figure 4(b), in ToR-level DC with high dynamic characteristics, DOTe performs worse than FIGRET in terms of both average performance and robustness.
- **TEAL.** TEAL is designed to train a fast and scalable TE scheme. It receives a traffic demand and outputs a network configuration specifically for this demand. However, when this network configuration is applied to future traffic demands, it tends to underperform.
- **FIGRET.** Our designed FIGRET achieves better results than previous TE methods, striking a better balance between average performance and robustness. For instance, compared to the TE scheme currently in production by Google’s Jupiter, FIGRET reduces the average MLU by 9%-34%. Against the state-of-the-art DOTe algorithm, specifically designed to lower MLU, FIGRET achieves a reduction in average MLU of 4.5% and 5.3% on ToR-level Facebook DB and ToR-level Facebook WEB, respectively, both characterized by high traffic dynamics. Even in stable topologies like Pod-level Datacenters, FIGRET does not underperform compared to DOTe. Simultaneously, we consider situations where the normalized MLU is greater than 2 as instances of severe congestion caused by inadequate network configuration. For the ToR-level Facebook DB, FIGRET exhibits a 41% lower incidence of severe congestion compared to DOTe, while for the ToR-level Facebook WEB, the reduction is 53.9%.

**Solver time.** We consider the solver time to consist of two parts: the calculation time required for applying each TE scheme to a new demand matrix, and the required precomputation time. Table 2 presents a comparison of the calculation time for different TE schemes. Table 2 lists four items: FIGRET, a Linear Programming (LP) approach that optimizes solely for expected traffic demands without applying sensitivity constraints, Desensitization-based TE, which addresses the optimization problem by imposing constraints to limit path sensitivity, and Oblivious & COPE, which are precomputed TE solutions not updated thereafter; hence, we only denote whether they can solve for the corresponding network. It is evident that a trained neural network, using matrix operations, can quickly compute a TE configuration. The comparison between LP and Des TE shows that adding constraints to the optimization problem to ensure robustness increases the solution time. However, by incorporating a penalty term into the neural network, we enhance robustness without increasing the latency. Compared to Des TE, FIGRET achieves a speed-up of 35× to 1800×.

Network	Calculation time (s)			
	FIGRET	LP	Des TE	OBL&Cope
GEANT (#Nodes 23)	0.002	0.04	0.07	Feasible
ToR DB (#Nodes 155)	0.005	1.60	5.00	Infeasible
ToR WEB (#Nodes 324)	0.009	7.30	17.00	Infeasible

**Table 2: Comparing the calculation time across various TE schemes. OBL represents Oblivious.**

Regarding the training time, since we employ a simple FCN architecture in FIGRET, the duration remains within an acceptable range. COPE and Demand-oblivious require substantial precomputation latency and a significant amount

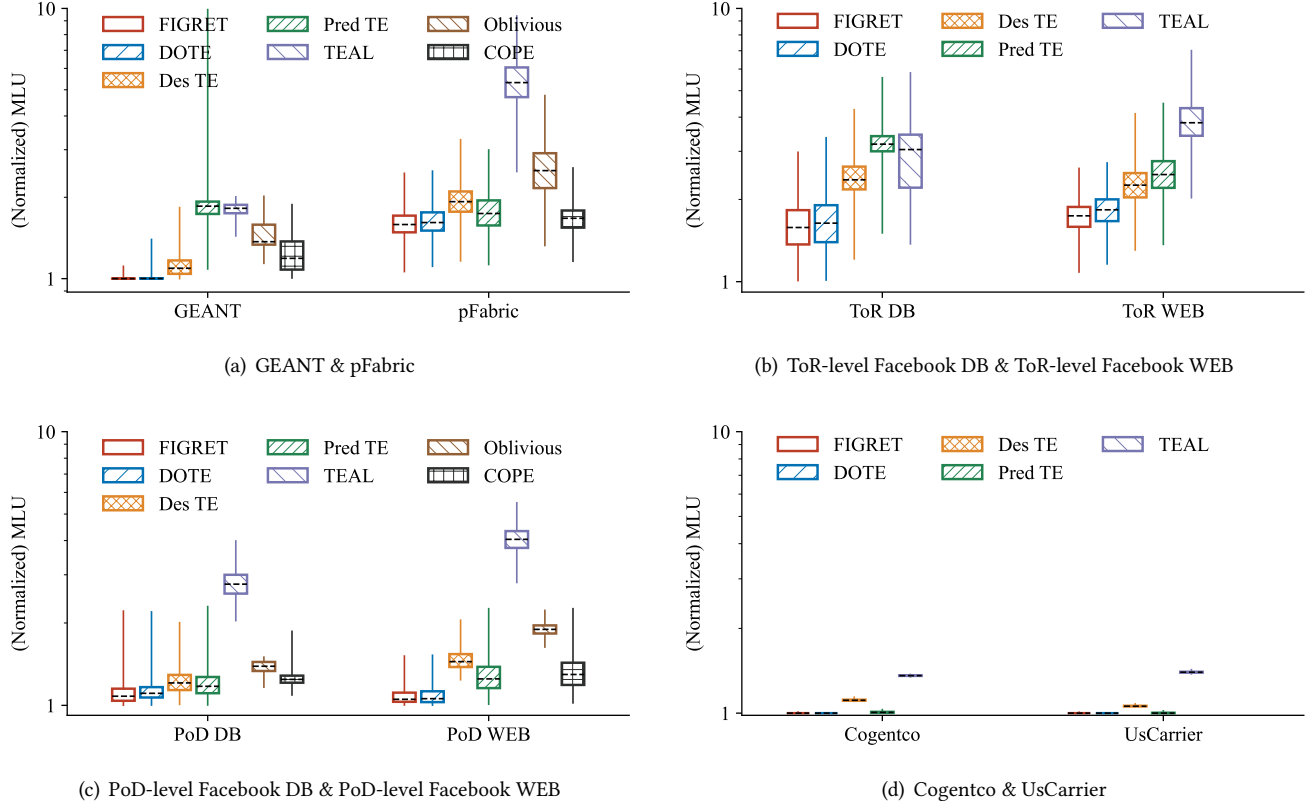


**Figure 4: Performance of FIGRET and baselines under the objective of minimizing max link utilization (MLU).**

of memory. Given a maximum runtime of 1 day and machine memory constraints, they only completed the topologies for GEANT, pFabric, and Pod-level DC. Past public results also show their applicability is limited to smaller topologies [36, 48]. Simultaneously, compared to TEAL, which employs reinforcement learning and graph neural networks, FIGRET also has advantages in terms of training time. Detailed data are presented in Table 8.

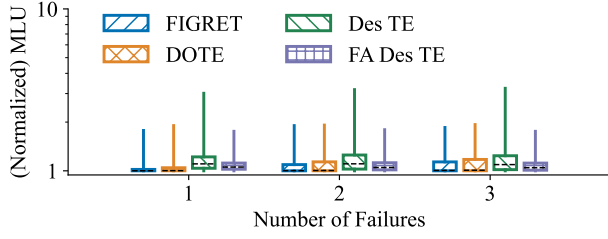
### 5.3 Coping with network failures

Figure 5 shows the performance of FIGRET, when different numbers of randomly selected links fail within the GEANT topology. We conduct a comparison between FIGRET, DOTE, Desensitization-based TE (Des TE), and Des TE that is also fault-aware, knowing the links that will fail in the *future* (FA Des TE). Their result is normalized against an oracle that possesses the best knowledge of both future demands and failures. Our results demonstrate that FIGRET achieves high resiliency to link failures. It outperforms both the DOTE and Des TE and is equally competitive with the FA Des TE, which has Oracle access to future failures. Our interpretation for

this is that first, compared to DOTE, FIGRET, by incorporating robustness constraints, ensures that the traffic load on a path does not become excessive, thereby mitigating the impact of link failures on performance. The reason why FIGRET can compete with the performance of FA Des TE is due to the more accurate  $D^{\text{expect}}$  obtained through deep learning and the benefits brought by fine-grained robustness enhancement, which offset the confusion induced by link failures. Our results on other topologies are presented in Appendix E. These results also exhibit similar characteristics.

### 5.4 Robustness to demand changes

**Temporary changes in traffic.** We test FIGRET for traffic variability. Our method for increasing variability is as follows: For each source-destination (SD) pair in the real traffic, we generate a traffic fluctuation using the Gaussian distribution  $N(\mu, \sigma^2)$  multiplied by a factor  $\alpha$ , where  $\mu = 0$  and  $\sigma$  is the standard deviation of the traffic demand  $d_{st}$ . Here,  $\alpha$  is chosen from the set  $\{0.2, 0.5, 1.0, 2.0\}$ , indicating the amplitude of the fluctuation. We observed how much the performance of FIGRET decreased after imposing sudden



**Figure 5: Coping with different numbers of random link failures on GEANT.**

traffic changes, compared to its performance without such changes. The results are summarized in Table 3. It can be observed that when the factor  $\alpha$  is relatively small, there is no significant decrease in FIGRET’s performance. At the same time, when the factor  $\alpha = 2$ , introducing noise twice that of  $N(0, \sigma_{Dsd, [1-T]}^2)$ , the performance decrease does not exceed 20%.

Network		Factor $\alpha$			
		0.2	0.5	1.0	2.0
PoD DB	average	-0.3%	0.2%	3.2%	9.8%
	90th Pct.	2.0%	3.0%	6.6%	16.7%
pFabric	average	0.2%	-0.6%	-1.8%	-2.9%
	90th Pct.	0.4%	0.5%	-1.0%	1.0%
ToR DB	average	1.6%	3.9%	8.9%	16.1%
	90th Pct.	0.8%	2.8%	4.5%	5.3%

**Table 3: Performance decline with increased Traffic Fluctuation. Negative values indicate no degradation.**

**Natural drift in traffic.** We test the impact of natural traffic shifts on FIGRET. In the aforementioned experiment, we sorted the data chronologically, using the first 75% for training and the latter 25% for testing. However, in this section, we conduct training separately with 0%-25%, 25%-50%, and 50%-75% of the data, followed by testing on the last 25%. This approach allows us to observe the performance decline compared to when 75% of the data is used for training. We focus on two aspects: firstly, the impact of training with less data on FIGRET’s performance; secondly, the effect of the update frequency on performance. The results are summarized in Table 4. It is observed that FIGRET’s performance remains largely unaffected even a long time after training completion (exceeding three times the total duration of the training data). To fully understand how traffic data evolves across time, we also visually analyzed the data distribution across various times in the topology, presented in Appendix F. The analysis indicates that neither PoD-level nor ToR-level data exhibit drastic changes in their traffic patterns over time. However, the shift effect at the ToR level is somewhat more

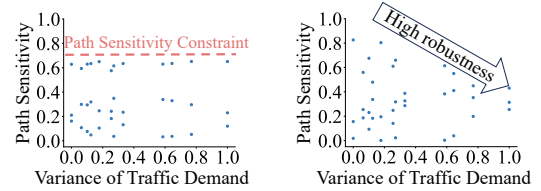
pronounced than at the PoD level. This corresponds with our results in Table 4. Through this analysis, we are inspired to recognize that the training of FIGRET does not necessarily need to be especially frequent.

Network		Training data time segments		
		0%-25%	25%-50%	50%-75%
PoD DB	average	-0.6%	-0.4%	-0.4%
	90th Pct.	-0.6%	-0.0%	-0.7%
pFabric	average	0.6%	0.9%	0.6%
	90th Pct.	1.3%	0.2%	1.0%
ToR DB	average	2.5%	2.0%	2.5%
	90th Pct.	3.0%	1.6%	1.6%

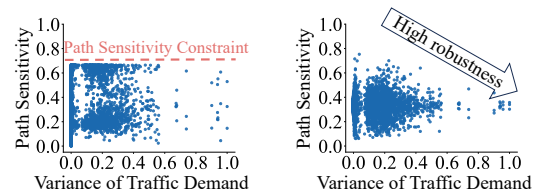
**Table 4: Performance decline with natural drift in traffic: negative values indicate no degradation.**

## 5.5 Interpreting FIGRET’s effectiveness

Beyond the impressive end-to-end results achieved by FIGRET, we aim to provide a high-level explanation that is easily understandable to humans. In this way, we aim to make network operators more inclined to implement FIGRET in practice.



(a) Desensitization-based TE, (b) FIGRET, PoD-level, Facebook PoD-level, Facebook DB cluster. DB cluster.



(c) Desensitization-based TE, (d) FIGRET, ToR-level, Facebook ToR-level, Facebook DB cluster. DB cluster.

**Figure 6: Compare the distribution of path sensitivities in Desensitization-based TE with FIGRET. Each point in the graph represents a path, with the x-axis indicating the variance of the traffic served by that path. The y-axis represents the average sensitivity of the path across all tested traffic demands.**

**Adaptive sensitivity analysis in FIGRET.** We evaluate FIGRET’s ability to ascertain reasonable sensitivity constraints,

as denoted by  $\mathcal{F}((s, t))$  in §4. We compare the network configurations of Google’s Desensitization-based TE and FIGRET, examining the relationship between path sensitivity and traffic characteristics. The results are presented in Figure 6. When creating Figure 6, we normalize the variance of the traffic on the x-axis. For the y-axis, in calculating path sensitivity, we normalize the capacity of the edges (considering the edge with the smallest capacity in the topology as 1). Furthermore, for the ToR level topology in Figure 6(c) and 6(d), with 155 nodes representing  $155 \times 154$  SD pairs and three paths per SD pair, there are a total of 1551543 paths. Due to the excessive number of points to plot, we uniformly select 10% of the SD pairs. From these results, we have the following observations: 1) For Desensitization-based TE, the path sensitivity of all paths, whether traffic is bursty or not, is constrained within a single path sensitivity constraint. 2) For FIGRET, path sensitivity settings depend on traffic characteristics: it’s dispersed for non-bursty and concentrated for bursty traffic. This enables detailed robustness analysis, achieving a better balance between performance and robustness to bursty traffic.

## 6 DISCUSSION

**Is deep learning essential for implementing the concept of fine-grained robustness enhancement?** In the design of FIGRET, we harness deep learning to devise a robustness enhancement scheme based on complex traffic characteristics and network topologies. However, considering that commercial network operators may be reluctant to overhaul their existing in-production TE systems completely, we discuss in this section whether slight modifications to the existing TE schemes, incorporating the principles of robustness enhancement, could result in better performance compared to the original TE schemes. To investigate this, we make slight modifications to the TE system currently in use by Google’s Jupiter. We discover that by designing simple heuristic-based  $\mathcal{F}$  path sensitivity constraint functions that align with fine-grained robustness concepts, the performance of TE algorithms can be improved. We employ linear functions that impose stricter constraints as traffic variability increases, and piecewise functions that divide traffic into more stable and bursty segments, applying looser and stricter constraints respectively. We validate that even such simple functions can improve the original TE’s performance to some extent (see Appendix C for more details).

Although it is feasible to directly apply fine-grained robustness enhancements to original systems, this approach encounters two significant issues: firstly, the use of LP methods for solving is notably slow. Secondly, manually configured functions often fall short of achieving optimal performance due to their inability to fully adapt to complex networks and

dynamic traffic demands. Given these considerations, this paper employs a method based on deep learning.

**When should FIGRET be retrained?** In this paper, FIGRET adopts a relatively simple periodic retraining approach, and as demonstrated in §5.4, retraining does not necessarily have to be particularly frequent. Thanks to FIGRET’s rapid training times, this periodic training approach can meet usage requirements. Alternative methods, such as retraining after detecting significant changes in Network Traffic Patterns or a certain degree of performance degradation, might more accurately determine the timing for retraining. However, we leave these considerations for future work.

## 7 RELATED WORK

**Traffic engineering.** Traffic engineering has been extensively studied in various scenarios, including wide area networks (WANs) [8, 9, 12, 18, 19, 23–26, 31, 39, 42, 48, 51, 54, 56, 57] and data center networks [5, 6, 11, 14–16, 37, 43]. Recently, SDN-based Traffic engineering has attracted considerable attention [2, 3, 13, 22, 23, 29, 32, 37, 53].

**Robustness-enhanced-based TE.** A major focus of research on TE is to improve the algorithm’s robustness in handling sudden traffic bursts. Oblivious TE [9] aims to enhance robustness by consistently considering the most congested scenario, optimizing for the worst-case MLU among all possible DMs. COPE [48] optimizes MLU across a set of DMs predicted by historical DMs while holding a worst-case MLU guarantee. Desensitization-based TE [37, 43], by introducing the concept of path sensitivity which characterizes the impact of traffic bursts on the path, aims to enhance robustness by optimizing the MLU while ensuring low path sensitivity across a historical set of DMs. Robustness-enhanced TE schemes typically exhibit coarse granularity by treating each source-destination pair in the traffic matrix equally. In contrast, FIGRET stands apart by employing fine-grained robustness enhancement, resulting in enhanced performance.

**Machine learning-based TE.** Machine learning-based TE can be broadly categorized into two classes. The first class is Demand Prediction-based TE [1, 30, 33, 34], where these methods utilize predictive models to initially compute an explicitly predicted next Traffic Matrix (TM). Subsequently, optimization is performed based on the predicted TM. The second class replaces explicit demand prediction with end-to-end optimization, directly mapping a recent historical window of TMs to TE configurations [36, 47]. Despite harnessing the powerful capabilities of deep learning to learn relationships between traffic flows, both of these classes overlook the consideration of unexpected traffic bursts.

## 8 CONCLUSION

In this work, we introduce FIGRET, a new design point for TE that enhances robustness in a fine-grained manner based on traffic characteristics. FIGRET employs path sensitivity to manage traffic bursts and utilizes a deep learning strategy with a well-designed loss function to produce TE solutions that consider robustness at a fine-grained level. Our experimental results demonstrate that FIGRET achieves an effective balance between average performance and robustness, resulting in high-quality TE solutions.

## REFERENCES

- [1] Firas Abuzaid, Srikanth Kandula, Behnaz Arzani, Ishai Menache, Matei Zaharia, and Peter Bailis. 2021. Contracting wide-area network topologies to solve flow problems quickly. In *18th USENIX Symposium on Networked Systems Design and Implementation (NSDI 21)*. 175–200.
- [2] Sugam Agarwal, Murali Kodialam, and TV Lakshman. 2013. Traffic engineering in software defined networks. In *2013 Proceedings IEEE INFOCOM*. IEEE, 2211–2219.
- [3] Ian F Akyildiz, Ahyoung Lee, Pu Wang, Min Luo, and Wu Chou. 2014. A roadmap for traffic engineering in SDN-OpenFlow networks. *Computer Networks* 71 (2014), 1–30.
- [4] Mohammad Al-Fares, Alexander Loukissas, and Amin Vahdat. 2008. A scalable, commodity data center network architecture. *ACM SIGCOMM computer communication review* 38, 4 (2008), 63–74.
- [5] Mohammad Al-Fares, Sivasankar Radhakrishnan, Barath Raghavan, Nelson Huang, Amin Vahdat, et al. 2010. Hedera: dynamic flow scheduling for data center networks.. In *Nsdi*, Vol. 10. San Jose, USA, 89–92.
- [6] Mohammad Alizadeh, Tom Edsall, Sarang Dharmapurikar, Ramanan Vaidyanathan, Kevin Chu, Andy Fingerhut, Vinh The Lam, Francis Matus, Rong Pan, Navindra Yadav, et al. 2014. CONGA: Distributed congestion-aware load balancing for datacenters. In *Proceedings of the 2014 ACM conference on SIGCOMM*. 503–514.
- [7] Mohammad Alizadeh, Shuang Yang, Milad Sharif, Sachin Katti, Nick McKeown, Balaji Prabhakar, and Scott Shenker. 2013. pfabric: Minimal near-optimal datacenter transport. *ACM SIGCOMM Computer Communication Review* 43, 4 (2013), 435–446.
- [8] David Applegate, Lee Breslau, and Edith Cohen. 2004. Coping with network failures: Routing strategies for optimal demand oblivious restoration. In *Proceedings of the joint international conference on Measurement and modeling of computer systems*. 270–281.
- [9] David Applegate and Edith Cohen. 2003. Making intra-domain routing robust to changing and uncertain traffic demands: Understanding fundamental tradeoffs. In *Proceedings of the 2003 conference on Applications, technologies, architectures, and protocols for computer communications*. 313–324.
- [10] Yossi Azar, Edith Cohen, Amos Fiat, Haim Kaplan, and Harald Racke. 2003. Optimal oblivious routing in polynomial time. In *Proceedings of the thirty-fifth annual ACM symposium on Theory of computing*. 383–388.
- [11] Theophilus Benson, Ashok Anand, Aditya Akella, and Ming Zhang. 2011. MicroTE: Fine grained traffic engineering for data centers. In *Proceedings of the seventh conference on emerging networking experiments and technologies*. 1–12.
- [12] Guillermo Bernárdez, José Suárez-Varela, Albert López, Bo Wu, Shihan Xiao, Xiangle Cheng, Pere Barlet-Ros, and Albert Cabellos-Aparicio. 2021. Is machine learning ready for traffic engineering optimization?. In *2021 IEEE 29th International Conference on Network Protocols (ICNP)*. IEEE, 1–11.
- [13] Jeremy Bogle, Nikhil Bhatia, Manya Ghobadi, Ishai Menache, Nikolaj Bjørner, Asaf Valadarsky, and Michael Schapira. 2019. TEAVAR: striking the right utilization-availability balance in WAN traffic engineering. In *Proceedings of the ACM Special Interest Group on Data Communication*. 29–43.
- [14] Peirui Cao, Shizhen Zhao, Min Yee The, Yunzhuo Liu, and Xinbing Wang. 2021. TROD: Evolving From Electrical Data Center to Optical Data Center. In *2021 IEEE 29th International Conference on Network Protocols (ICNP)*. IEEE, 1–11.
- [15] Peirui Cao, Shizhen Zhao, Dai Zhang, Zhuotao Liu, Mingwei Xu, Min Yee Teh, Yunzhuo Liu, Xinbing Wang, and Chenghu Zhou. 2023. Threshold-based routing-topology co-design for optical data center. *IEEE/ACM Transactions on Networking* (2023).
- [16] Li Chen, Justinas Lingys, Kai Chen, and Feng Liu. 2018. Auto: Scaling deep reinforcement learning for datacenter-scale automatic traffic optimization. In *Proceedings of the 2018 conference of the ACM special interest group on data communication*. 191–205.
- [17] Marco Chiesa, Gábor Rétvári, and Michael Schapira. 2016. Lying your way to better traffic engineering. In *Proceedings of the 12th International Conference on emerging Networking EXperiments and Technologies*. 391–398.
- [18] Anwar Elwalid, Cheng Jin, Steven Low, and Indra Widjaja. 2001. MATE: MPLS adaptive traffic engineering. In *Proceedings IEEE INFOCOM 2001. Conference on Computer Communications. Twentieth Annual Joint Conference of the IEEE Computer and Communications Society (Cat. No. 01CH37213)*, Vol. 3. IEEE, 1300–1309.
- [19] Bernard Fortz and Mikkel Thorup. 2000. Internet traffic engineering by optimizing OSPF weights. In *Proceedings IEEE INFOCOM 2000. conference on computer communications. Nineteenth annual joint conference of the IEEE computer and communications societies (Cat. No. 00CH37064)*, Vol. 2. IEEE, 519–528.
- [20] LLC Gurobi Optimization. 2021. Gurobi optimizer reference manual. (2021).
- [21] Geoffrey E Hinton and Sam Roweis. 2002. Stochastic neighbor embedding. *Advances in neural information processing systems* 15 (2002).
- [22] Chi-Yao Hong, Srikanth Kandula, Ratul Mahajan, Ming Zhang, Vijay Gill, Mohan Nanduri, and Roger Wattenhofer. 2013. Achieving high utilization with software-driven WAN. In *Proceedings of the ACM SIGCOMM 2013 Conference on SIGCOMM*. 15–26.
- [23] Sushant Jain, Alok Kumar, Subhasree Mandal, Joon Ong, Leon Poutievski, Arjun Singh, Subbaiah Venkata, Jim Wanderer, Junlan Zhou, Min Zhu, et al. 2013. B4: Experience with a globally-deployed software defined WAN. *ACM SIGCOMM Computer Communication Review* 43, 4 (2013), 3–14.
- [24] Wenjie Jiang, Rui Zhang-Shen, Jennifer Rexford, and Mung Chiang. 2009. Cooperative content distribution and traffic engineering in an ISP network. In *Proceedings of the eleventh international joint conference on Measurement and modeling of computer systems*. 239–250.
- [25] Srikanth Kandula, Dina Katabi, Bruce Davie, and Anna Charny. 2005. Walking the tightrope: Responsive yet stable traffic engineering. *ACM SIGCOMM Computer Communication Review* 35, 4 (2005), 253–264.
- [26] Srikanth Kandula, Ishai Menache, Roy Schwartz, and Spandana Raj Babbula. 2014. Calendaring for wide area networks. In *Proceedings of the 2014 ACM conference on SIGCOMM*. 515–526.
- [27] Diederik P Kingma and Jimmy Ba. 2014. Adam: A method for stochastic optimization. *arXiv preprint arXiv:1412.6980* (2014).
- [28] Simon Knight, Hung X Nguyen, Nickolas Falkner, Rhys Bowden, and Matthew Roughan. 2011. The internet topology zoo. *IEEE Journal on Selected Areas in Communications* 29, 9 (2011), 1765–1775.
- [29] Alok Kumar, Sushant Jain, Uday Naik, Anand Raghuraman, Nikhil Kasinadhuni, Enrique Cauich Zermeno, C Stephen Gunn, Jing Ai, Björn Carlin, Mihai Amarandei-Stavila, et al. 2015. BwE: Flexible,

- hierarchical bandwidth allocation for WAN distributed computing. In *Proceedings of the 2015 ACM Conference on Special Interest Group on Data Communication*. 1–14.
- [30] Praveen Kumar, Chris Yu, Yang Yuan, Nate Foster, Robert Kleinberg, and Robert Soulé. 2018. YATES: Rapid prototyping for traffic engineering systems. In *Proceedings of the Symposium on SDN Research*. 1–7.
- [31] Praveen Kumar, Yang Yuan, Chris Yu, Nate Foster, Robert Kleinberg, Petr Lapukhov, Chiun Lin Lim, and Robert Soulé. 2018. {Semi-Oblivious} Traffic Engineering: The Road Not Taken. In *15th USENIX Symposium on Networked Systems Design and Implementation (NSDI 18)*. 157–170.
- [32] Hongqiang Harry Liu, Srikanth Kandula, Ratul Mahajan, Ming Zhang, and David Gelernter. 2014. Traffic engineering with forward fault correction. In *Proceedings of the 2014 ACM Conference on SIGCOMM*. 527–538.
- [33] Pooria Namyar, Behnaz Arzani, Ryan Beckett, Santiago Segarra, Himanshu Raj, and Srikanth Kandula. 2022. Minding the gap between fast heuristics and their optimal counterparts. In *Proceedings of the 21st ACM Workshop on Hot Topics in Networks*. 138–144.
- [34] Deepak Narayanan, Fiodar Kazhamiaka, Firas Abuzaid, Peter Kraft, Akshay Agrawal, Srikanth Kandula, Stephen Boyd, and Matei Zaharia. 2021. Solving large-scale granular resource allocation problems efficiently with pop. In *Proceedings of the ACM SIGOPS 28th Symposium on Operating Systems Principles*. 521–537.
- [35] Adam Paszke, Sam Gross, Francisco Massa, Adam Lerer, James Bradbury, Gregory Chanan, Trevor Killeen, Zeming Lin, Natalia Gimelshein, Luca Antiga, et al. 2019. Pytorch: An imperative style, high-performance deep learning library. *Advances in neural information processing systems* 32 (2019).
- [36] Yarin Perry, Felipe Vieira Frujeri, Chaim Hoch, Srikanth Kandula, Ishai Menache, Michael Schapira, and Aviv Tamar. 2023. {DOTE}: Rethinking (Predictive){WAN} Traffic Engineering. In *20th USENIX Symposium on Networked Systems Design and Implementation (NSDI 23)*. 1557–1581.
- [37] Leon Poutievski, Omid Mashayekhi, Joon Ong, Arjun Singh, Mukarram Tariq, Rui Wang, Jianan Zhang, Virginia Beauregard, Patrick Conner, Steve Gribble, et al. 2022. Jupiter evolving: transforming google’s datacenter network via optical circuit switches and software-defined networking. In *Proceedings of the ACM SIGCOMM 2022 Conference*. 66–85.
- [38] Matthew Roughan, Albert Greenberg, Charles Kalmanek, Michael Rumsewicz, Jennifer Yates, and Yin Zhang. 2002. Experience in measuring backbone traffic variability: Models, metrics, measurements and meaning. In *Proceedings of the 2nd ACM SIGCOMM Workshop on Internet Measurement*. 91–92.
- [39] Matthew Roughan, Mikkel Thorup, and Yin Zhang. 2003. Traffic engineering with estimated traffic matrices. In *Proceedings of the 3rd ACM SIGCOMM Conference on Internet Measurement*. 248–258.
- [40] Arjun Roy, Hongyi Zeng, Jasmeet Bagga, George Porter, and Alex C Snoeren. 2015. Inside the social network’s (datacenter) network. In *Proceedings of the 2015 ACM Conference on Special Interest Group on Data Communication*. 123–137.
- [41] Ankit Singla, Chi-Yao Hong, Lucian Popa, and P Brighten Godfrey. 2012. Jellyfish: Networking data centers randomly. In *9th USENIX Symposium on Networked Systems Design and Implementation (NSDI 12)*. 225–238.
- [42] Martin Suchara, Dahai Xu, Robert Doverspike, David Johnson, and Jennifer Rexford. 2011. Network architecture for joint failure recovery and traffic engineering. *ACM SIGMETRICS Performance Evaluation Review* 39, 1 (2011), 97–108.
- [43] Min Yee Teh, Shizhen Zhao, Peirui Cao, and Keren Bergman. 2020. COUDER: robust topology engineering for optical circuit switched data center networks. *arXiv preprint arXiv:2010.00090* (2020).
- [44] Min Yee Teh, Shizhen Zhao, Peirui Cao, and Keren Bergman. 2022. Enabling quasi-static reconfigurable networks with robust topology engineering. *IEEE/ACM Transactions on Networking* (2022).
- [45] Renata Teixeira, Sharad Agarwal, and Jennifer Rexford. 2005. BGP routing changes: Merging views from two ISPs. *ACM SIGCOMM Computer Communication Review* 35, 5 (2005), 79–82.
- [46] Steve Uhlig, Bruno Quoitin, Jean Lepropre, and Simon Balon. 2006. Providing public intradomain traffic matrices to the research community. *ACM SIGCOMM Computer Communication Review* 36, 1 (2006), 83–86.
- [47] Asaf Valadarsky, Michael Schapira, Dafna Shahaf, and Aviv Tamar. 2017. Learning to route. In *Proceedings of the 16th ACM workshop on hot topics in networks*. 185–191.
- [48] Hao Wang, Haiyong Xie, Lili Qiu, Yang Richard Yang, Yin Zhang, and Albert Greenberg. 2006. COPE: Traffic engineering in dynamic networks. In *Proceedings of the 2006 conference on Applications, technologies, architectures, and protocols for computer communications*. 99–110.
- [49] Yue Wang, Yongbin Sun, Ziwei Liu, Sanjay E Sarma, Michael M Bronstein, and Justin M Solomon. 2019. Dynamic graph cnn for learning on point clouds. *ACM Transactions on Graphics (tog)* 38, 5 (2019), 1–12.
- [50] Kuai Xu, Zhi-Li Zhang, and Supratik Bhattacharyya. 2005. Profiling internet backbone traffic: behavior models and applications. *ACM SIGCOMM Computer Communication Review* 35, 4 (2005), 169–180.
- [51] Zhiying Xu, Francis Y Yan, Rachee Singh, Justin T Chiu, Alexander M Rush, and Minlan Yu. 2023. Teal: Learning-Accelerated Optimization of WAN Traffic Engineering. In *Proceedings of the ACM SIGCOMM 2023 Conference*. 378–393.
- [52] Rex Ying, Ruining He, Kaifeng Chen, Pong Eksombatchai, William L Hamilton, and Jure Leskovec. 2018. Graph convolutional neural networks for web-scale recommender systems. In *Proceedings of the 24th ACM SIGKDD international conference on knowledge discovery & data mining*. 974–983.
- [53] Nicu Florin Zaicu, Matthew Luckie, Richard Nelson, and Marinho Barcellos. 2021. Helix: Traffic Engineering for Multi-Controller SDN. In *Proceedings of the ACM SIGCOMM Symposium on SDN Research (SOSR)*. 80–87.
- [54] Hong Zhang, Kai Chen, Wei Bai, Dongsu Han, Chen Tian, Hao Wang, Haibing Guan, and Ming Zhang. 2015. Guaranteeing deadlines for inter-datacenter transfers. In *Proceedings of the Tenth European Conference on Computer Systems*. 1–14.
- [55] Hengrui Zhang, Zhongming Yu, Guohao Dai, Guyue Huang, Yufei Ding, Yuan Xie, and Yu Wang. 2022. Understanding gnn computational graph: A coordinated computation, io, and memory perspective. *Proceedings of Machine Learning and Systems* 4 (2022), 467–484.
- [56] Yin Zhang and Zihui Ge. 2005. Finding critical traffic matrices. In *2005 International Conference on Dependable Systems and Networks (DSN’05)*. IEEE, 188–197.
- [57] Zhizhen Zhong, Manya Ghobadi, Alaa Khaddaj, Jonathan Leach, Yiting Xia, and Ying Zhang. 2021. ARROW: restoration-aware traffic engineering. In *Proceedings of the 2021 ACM SIGCOMM 2021 Conference*. 560–579.



## APPENDIX

### A NOTATION TABLE

In this section, we tabulate the notations in Table 5.

Notation	Description
$G(V, E, c)$	Network topology, $V$ is vertex set, $E$ is edge set, and $c$ assigns capacities to edges
$D$	Demand matrix, where $D_{ij}$ denotes the traffic from $i$ to $j$
$P$	Network paths, where $P_{sd}$ denotes the set of network paths through which source $s$ communicates with destination $d$
$C_p$	The capacity of path $p$
$r_p$	The split ratio of the traffic demand from $s$ to $d$ forwarded along path $p$
$\mathcal{R}$	TE configuration
$M(\mathcal{R}, D)$	MLU in the network given $D$ and $\mathcal{R}$
$\Delta$	The set representing mismatch
$\mathcal{S}_p$	Path sensitivity for path $p$
$\mathcal{S}_{sd}^{\max}$	Maximum path sensitivity among all paths in $P_{st}$
$\mathcal{F}$	Function for path sensitivity constraints
$\pi_\theta$	The mapping function from DNN inputs to outputs, and $\theta$ denotes the DNN's weight
$H$	Window length, representing the number of historical traffic demands in the DNN input
$\mathcal{L}(\mathcal{R}_t, D_t)$	Loss function
$\sigma_{D_{sd}, [1-T]}^2$	The variance of traffic demands $D_{sd}$ within the time range from 1 to $T$

Table 5: Notations used in this paper

### B TE OPTIMIZATION FORMULATION

In this section, we formulate the TE optimization problem. Given a network  $G(V, E, c)$  and traffic demand  $D$ , to find an optimal TE configuration which specifies a split ratio  $r_p$  for each path  $p \in P_{st}$ , where  $r_p$  represents the fraction of the traffic demand from  $s$  to  $t$  forwarder along path  $p$ , the optimization formulation shown in Equation 9 can be established.

$$\begin{aligned}
 & \underset{\mathcal{R}}{\text{minimize}} && \max_{e \in E} \frac{f_e}{c(e)} \\
 & \text{subject to} && \sum_{p \in P_{st}} r_p = 1, \forall s, t \in V \\
 & && \sum_{s, t \in V, p \in P_{st}, e \in p} D_{st} \times r_p = f_e, \forall e \in E
 \end{aligned} \tag{9}$$

Our work, however, focuses on realistic scenarios where TE schemes must select configurations on the realistic scenario in which the traffic demand is not known beforehand.

### C HEURISTIC SELECTION OF $\mathcal{F}$

In this section, we integrate the Desensitization-based TE scheme in Google's Jupiter Evolving [37], replacing its fixed path sensitivity constraints with a heuristically selected function  $\mathcal{F} : (s, t) \rightarrow \mathbb{R}^+$ . As discussed in §4, for stable traffic, we apply lenient sensitivity constraints, whereas, for highly bursty traffic, we impose stringent constraints. We use traffic variance as an indicator of traffic burstiness. Therefore, the path sensitivity constraints should become increasingly stringent as the path variance increases, meaning the maximum allowable path sensitivity should decrease correspondingly. We experiment with two heuristic functions: 1) Linear function, and 2) Piecewise function.

#### C.1 Linear function

The function we have selected is illustrated in Figure 7. Using a linear function, we arrange the traffic variance for all SD pairs in ascending order and assign varying path sensitivity constraints based on different orders. The *Max* and *Min* values in the Figure can be arbitrarily chosen, but ensuring that a solution is feasible when selecting *Min* is crucial. For instance, if there are  $n$  paths serving this SD pair, each with capacity of 1, it is required that  $r_p \leq \text{Min}$  and  $\sum_{i=1}^n r_i = 1$ . In this scenario, *Min* should not be less than  $\frac{1}{n}$ ; otherwise, the problem becomes unsolvable.

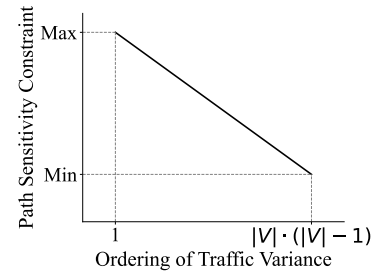
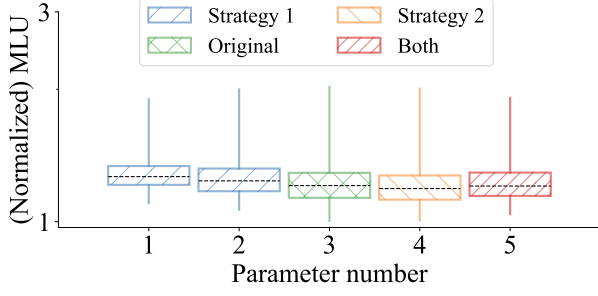


Figure 7: Illustrating the function  $\mathcal{F}$  selected by Linear function.

We conduct tests using varying *Min* and *Max* parameters, which are listed in Table 6. Strategy 1 refers to the implementation of stricter path sensitivity restrictions. In contrast, Strategy 2 involves relaxing the path sensitivity restrictions for more stable flows. Meanwhile, Strategy 3 suggests a combination approach: it proposes enforcing stricter path sensitivity restrictions on sudden or bursty flows while simultaneously relaxing these restrictions for stable flows.



**Figure 8: Comparing the TE quality under different parameter settings in Linear function. The parameter number on the x-axis corresponds to the numbering in Table 6**

For ease of numerical representation, we have normalized the capacities of all paths in the graph, setting the smallest capacity to 1, with other capacities calculated proportionally.

	Strategy 1		Original	Strategy 2	Both
Number	1	2	3	4	5
Min	1/3↓	1/3↓	2/3	2/3	1/3↓
Max	1/2↓	2/3	2/3	5/6↑	5/6↑

**Table 6: The parameters selected for the Linear function. ‘Original’ refers to the fixed path sensitivity constraint of the Desensitization-based TE.**

We apply the parameters listed in Table 6 and conduct tests on the PoD-level Facebook DB. The results are summarized in Figure 8. As shown in Figure 8, the application of Strategy 1, which involves imposing stricter path sensitivity constraints (as in the case of the group {1,2,3}), leads to an enhanced capability to handle bursty traffic. On the other hand, with the implementation of Strategy 2, an improvement in average performance is observed, as demonstrated by the comparison of groups {3,4}.

## C.2 Piecewise function

The function we have selected for our analysis is depicted in Figure 9. It utilizes a piecewise approach to define constraints on path sensitivity, following the same x-axis and y-axis interpretations as shown in Figure 7. We specifically chose a piecewise function for this purpose. We introduce a breakpoint within the function to distinguish between stable and bursty traffic conditions. For traffic variances that fall below this breakpoint, indicative of stable flow, the path sensitivity constraints are comparatively relaxed. In contrast,

for traffic variances that exceed this breakpoint, representing bursty flow, the constraints are tighter and more rigorous.

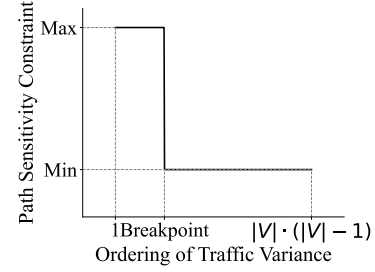


**Figure 9: Illustrating the function  $\mathcal{F}$  selected by Piecewise function.**

We employ various parameters to demonstrate the impact of different parameter settings on the results. In this function, the parameters available for selection include *Min*, *Max*, and *breakpoint*. Our parameter settings are presented in Table 7. For ease of numerical representation, we have normalized the capacities of all paths in the graph, setting the smallest capacity to 1, with other capacities calculated proportionally. Additionally, we represent the value of the breakpoint in terms of its proportion rather than as an absolute number. For example, breakpoint=0.8 signifies that the first 80% of the flow is relatively stable, while the latter 20% comprises bursty traffic.

	Strict Constraint			Original	Relaxed Constraint		
Number	1	2	3	4	5	6	7
Min	1/2↓	1/2↓	1/2↓	2/3	2/3	2/3	2/3
Max	2/3	2/3	2/3	2/3	5/6↑	5/6↑	5/6↑
Breakpoint	0.5	0.65	0.8	\	0.5	0.65	0.8

**Table 7: The parameters selected for the Piecewise function. ‘Original’ refers to the fixed path sensitivity constraint of the Desensitization-based TE.**

In our study, we conducted a series of tests on the parameters listed in Table 7 on PoD-level Facebook DB, with the results summarized in Figure 10. As illustrated in the figure, with fixed values of *Min* and *Max*, a larger *Breakpoint* setting enhances the average performance of TE methods. This trend is evident in groups {1,2,3} and {5,6,7}, where an increase in *Breakpoint* corresponds to a lower average performance boxplot. Conversely, with a constant *Breakpoint*, maintaining *Max* while reducing *Min* enhances the TE methods’ ability to manage bursty traffic, as shown in the comparison of group {1,4}. Similarly, fixing *Min* while increasing *Max* leads to better average performance of TE methods, as observed in the comparison between groups {4,5}.

These findings align with intuitive expectations: a higher proportion of stable traffic or more lenient path sensitivity constraints for stable traffic result in improved average algorithm performance. Conversely, a lower proportion of stable traffic with stricter constraints for bursty traffic enhances the algorithm’s ability to handle sudden bursts.

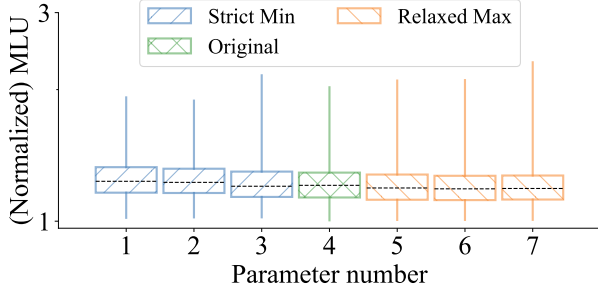


**Figure 10: Comparing the TE quality under different parameter settings in Piecewise function. The parameter number on the x-axis corresponds to the numbering in Table 7.**

### C.3 Summary

This section demonstrates that by implementing fine-grained robustness enhancement strategies into Google’s TE using simple heuristic functions, we can achieve varying effects through parameter adjustments, thereby enhancing the original TE algorithm’s capabilities. Our application of deep learning in FIGRET aims to identify the function form and parameters for fine-grained robustness enhancement as effectively as possible, while also speeding up the TE solution process.

## D FIGRET IMPLEMENTATION DETAILS

While we have chosen FCN among FCN, CNN, and GNN for our application, this does not imply that TE problems must exclusively use FCNs. More sophisticated and advanced network architectures can be further explored.

### D.1 No need for GNN

The mapping between TE configuration and Maximum Link Utilization (MLU) can be represented using Function 1. As seen from Function 1, this mapping can be established through simple matrix operations.

### D.2 The inappropriateness of CNN

In Figure 11, there is a source  $s$  and three destinations  $t_1, t_2, t_3$ , with a convolution kernel size of 2. This kernel aims to extract *local* information of length 2 from the traffic demands. However, extracting local information between  $d_1, d_2$  and  $d_2, d_3$  proves ineffective because  $p_{st_1}$  and  $p_{st_2}$ , as well as  $p_{st_2}$  and

---

#### Function 1: Mapping traffic configurations to MLU

---

- 1  $G = (V, E, c)$  // Graph that models the network topology
  - 2  $\Omega = \{(i, j) | i \in V, j \in V, i \neq j\}$  // the set of all source-destination (SD) pairs
  - 3  $\Phi = \bigcup_{s,t \in \Omega} P_{st}$  // the set of all paths
  - 4  $SDtoPath^{|\Omega| \times |\Phi|}$  // Signifies whether path  $j$  serves the SD pair  $i$ .  $SDtoPath_{i,j} = 1$  if path  $j$  serves SD pair  $i$ , 0 otherwise
  - 5  $PathtoEdge^{|\Phi| \times |E|}$  // Signifies whether path  $i$  contains edge  $j$ .  $PathtoEdge_{i,j} = 1$  if edge  $j \in$  path  $i$ , 0 otherwise
  - 6  $\mathcal{R}^{|\Phi| \times 1}$  // Network configuration yields the split ratios for all paths
  - 7  $C^{|E| \times 1}$  // vector representing link capacities
  - 8  $DM_{|\Omega| \times 1}$  // Flatten traffic demand matrix  
/\* Compute MLU form  $\mathcal{R}$ .  $\times$  for matrix multiplication;  
 $\odot$  for element-wise (Hadamard) multiplication \*/
  - 9  $FlowOnPath^{|\Phi| \times 1} = SDtoPath^T \times DM \odot \mathcal{R}$   
//  $(|\Phi|, |\Omega|) \times (|\Omega|, 1) \odot (|\Phi|, 1)$ , calculate the flow on each path
  - 10  $FlowOnEdge^{|E| \times 1} = PathtoEdge^T \times FlowOnPath$   
//  $(|E|, |\Phi|) \times (|\Phi|, 1)$ , calculate the flow on each edge
  - 11  $MLU = \text{Max}(FlowOnEdge/C)$
- 

$p_{st_3}$ , do not share a common edge. Conversely,  $p_{st_1}$  and  $p_{st_3}$  do share a common edge, and their traffic demands should be considered jointly. This limitation cannot be addressed by such convolution layers that are designed to extract local information. Unlike image data, which CNNs excel at handling due to the localized relevance of information, TE problems do not exhibit a distinct need for extracting local information because traffic demands within a convolutional locality may not necessarily pass through a common edge, making the use of convolution for local information extraction minimally effective. Therefore, in our model design, we chose not to incorporate convolutional layers. Instead, we opted for directly utilizing fully connected layers.

### D.3 Drawbacks of Using RL

Reinforcement learning is extensively applied in Traffic Engineering (TE), as exemplified by TEAL [51]. This method learns strategies for achieving objectives in complex environments through trial and error. However, it often comes with high computational complexity and sensitivity to parameter settings. In TE, the relationship between policies—TE

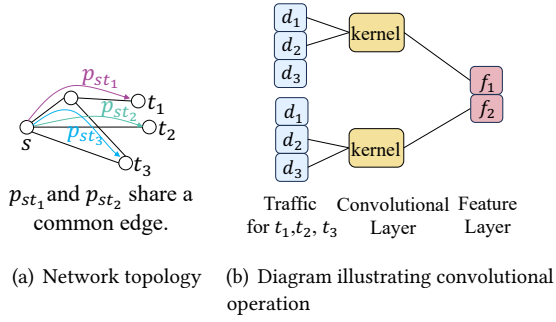


**Figure 11: Diagram illustrating the convolution operation in TE. Traffic demands for paths that share a common edge need to be considered jointly due to their potential impact on each other. In contrast, for paths without a shared edge, jointly considering their traffic demands is ineffective.**

configurations and the objective of minimizing link utilization (MLU) is quite explicit and can be directly expressed. In such relatively simple scenarios, reinforcement learning may not be the most optimal choice. Under these circumstances, it's unnecessary to undergo the complex exploration and trial-and-error adjustments typical of reinforcement learning. Instead, direct application of gradient descent methods could be more effective.

In Table 8, we present a comparison of the training times for FIGRET and TEAL, which involve GNN and reinforcement learning, as well as the precomputation time for Oblivious and COPE. It is evident that as the network topology scales up, FIGRET's precomputation time offers a greater advantage.

Network	Precomp. time (s)			
	FIGRET	TEAL	OBL	COPE
GEANT (#Nodes 23)	150	1500	100	1000
ToR DB (#Node 155)	500	7000	-	-
ToR WEB (#Node 324)	1500	20000	-	-

**Table 8: Comparing the precomputation time, OBL represents Oblivious. A '-' indicates that the corresponding TE scheme could not be solved within the constraints of the maximum memory of the given machine and a solving time limit of one day.**

#### D.4 Implementing FIGRET

**DNN architecture.** Similar to DOTE, except for the input and output layers, FIGRET uses five fully connected neural network layers with 128 neurons each and employs ReLU(x)

activation, except for the output layer, which uses Sigmoid(x). **Optimizer.** During the training process, FIGRET employs the Adam optimizer [27] for stochastic gradient descent.

#### E ADDITIONAL LINK FAILURE RESULTS

In this section, we present the results from evaluating link failures on pFabric and ToR-level DC Facebook DB, as shown in Figures 12 and 13. As can be seen in Figure 13, when the network traffic demands exhibit high dynamics, the current TE scheme in Google's Jupiter, even with the knowledge of which links are going to fail, fails to achieve satisfactory results.

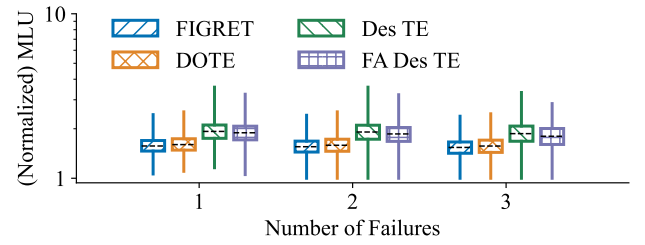


**Figure 12: Coping with different numbers of random link failures on pFabric.**

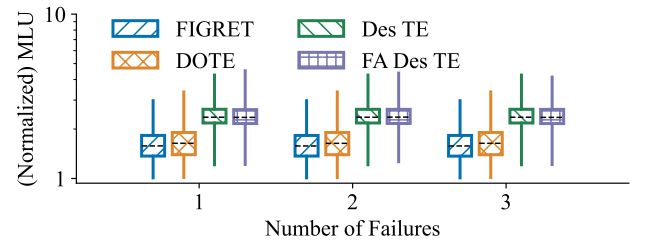


**Figure 13: Coping with different numbers of random link failures on ToR-level Facebook DB.**

#### F VISUALIZATION OF TRAFFIC DEMANDS

To visually demonstrate the extent of traffic data migration over time, we conduct a visualization analysis of traffic demands from both the PoD-level Facebook DB and the ToR-level Facebook DB using the t-distributed stochastic neighbor embedding (t-SNE) method [21] in this section. We analyze their traffic from 0% to 100% using t-SNE and compare the differences in the intervals of 0% – 25%, 25% – 50%, 50% – 75%, and 75% – 100%. The 2-dimensional t-SNE components are plotted in Figure 14 and Figure 15.

From the results, we observe the following:

- Compared to the PoD-level data, the ToR-level data is more dispersed, indicating a higher dynamism in ToR-level traffic data.
- Both ToR-level and PoD-level data exhibit a single cluster formation in the t-SNE plots, suggesting their traffic patterns do not undergo drastic changes over time.
- While the PoD-level data remains very similar across all four-time segments, the ToR-level data shows some variations.

These observations are consistent with our evaluation results, indicating firstly that TE is more challenging at the ToR-level (§5.2) and, secondly, that FIGRET’s robustness to time drift performs well at both levels (§5.4). Moreover, the impact of time drift on FIGRET’s effectiveness is greater at the ToR-level (§5.4).

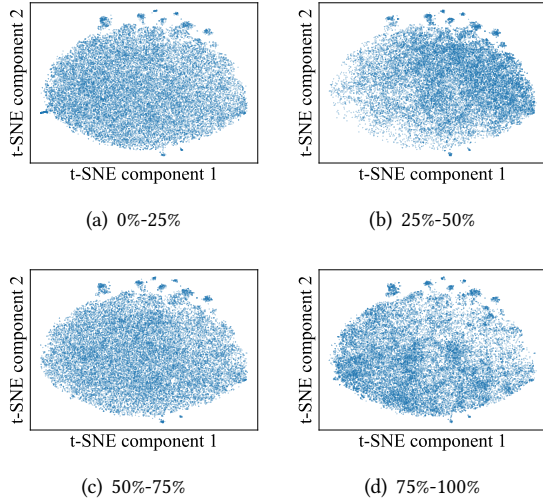


**Figure 14: Visualizing Traffic Demands of the PoD-level Facebook DB using the t-SNE Method.**

## G A CLOSER LOOK AT THE DRAWBACKS OF EXISTING TE SCHEMES

### G.1 Objective mismatch in Demand-prediction-based TE

In demand-prediction-based TE, a notable mismatch exists between the objective of accurately predicting future traffic and minimizing the MLU [36]. This mismatch primarily arises from the influence of network topology on MLU, indicating that traffic demands exert varied impacts on MLU. For instance, traffic traversing paths with higher capacity tends to have a lesser effect on MLU. Similarly, traffic flowing through paths without shared edges with other paths will

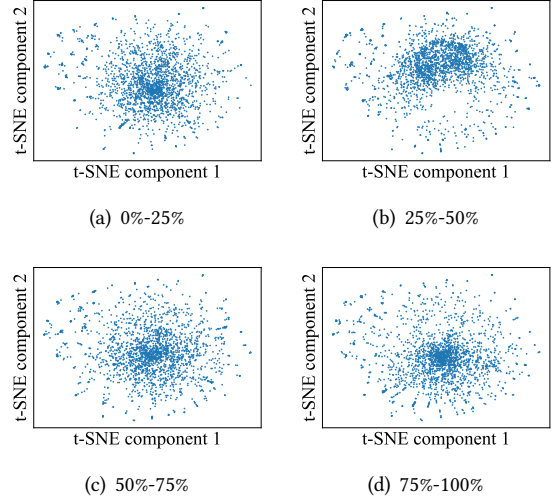
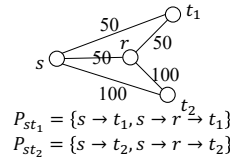


**Figure 15: Visualizing Traffic Demands of the ToR-level Facebook DB using the t-SNE Method.**

also impact MLU to a lesser degree. An example illustrating this concept is provided in Figure 16.



(a) In the network topology, where numbers on edges indicate link capacity, traffic demands of  $d_1$  and  $d_2$  need to be sent from  $s$  to  $t_1$  and  $s$  to  $t_2$ , respectively.

Predicted ( $d_1, d_2$ )	Split ratio ( $r_{[s \rightarrow t_1]}, r_{[s \rightarrow t_2]}$ )	MLU
(50, 60)	(11/20, 11/12)	0.66
(60, 50)	(1/2, 1)	0.6
Upcoming Demand: (60, 60)		

(b) An example concerning predicted traffic, where the split ratios are only specified for the paths  $s \rightarrow t_1$  and  $s \rightarrow t_2$ , with the split ratios for the other two paths being 1 minus the corresponding split ratios.

**Figure 16: An example demonstrating the mismatch between achieving accurate traffic predictions and minimizing MLU.** Two predicted demands achieve the same level of prediction accuracy (with identical mean-square-error values). However, the optimal split ratios derived from these two traffic predictions lead to different MLUs. Incorrect predictions of the traffic from  $s$  to  $t_2$  have a lesser impact on MLU. This is due to the larger capacity of the path from  $s$  to  $t_2$ .

### G.2 Limited gains from window expansion

Deep learning approaches demonstrate powerful capabilities in using information within a window to obtain a better  $D^{\text{expect}}$ . Therefore, in this section, we consider whether,



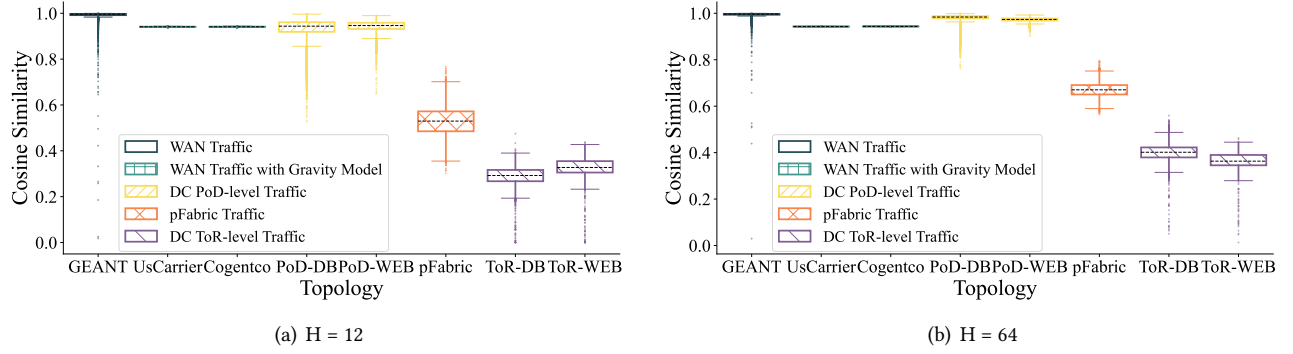
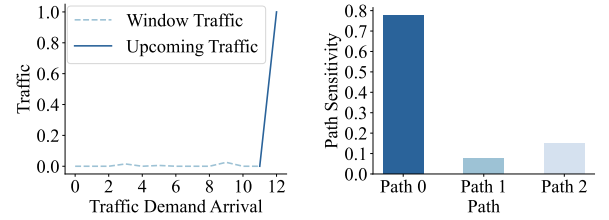


**Figure 17: Cosine similarity analysis using a window of  $H$  historical TMs vs. the currently-seen TM.**

under the premise of sufficient computational power and memory, expanding the window size could make  $D^{\text{expect}}$  highly accurate and prevent mis-predictions, thereby eliminating the need to consider sudden traffic changes. Using an analysis method similar to §5, we examine the cosine similarity between upcoming traffic and traffic from the past  $H$  time windows, where  $H$  is increased to 64. The results are summarized in Figure 17. However, the results indicate that, regardless of whether in stable or bursty network types, the cosine similarity does not significantly increase compared to when  $H$  is 12, suggesting that expanding the window size is *ineffective* in avoiding sudden traffic changes.

Due to the limited information within the window, DOTE, which solely relies on window-based information and prioritizes MLU, may result in suboptimal configurations. An example is shown in Figure 18, which illustrates an inadequate network configuration by DOTE on the ToR-level Facebook DB (with an Omniscient-normalized MLU of 2.86). We selected the SD pair responsible for the MLU, and as seen in Figure 18(a), the traffic on this SD pair was consistently

stable at a relatively low value. Therefore, DOTE assigned a configuration for this SD pair involving paths with high path sensitivity. However, in the next time snapshot, the SD pair burst unexpectedly, significantly impacting the highly sensitive paths, leading to high MLU.



(a) The arrival scenario of the traffic (b) Path sensitivity of this SD pair. for a SD pair.

**Figure 18: Showcasing the limitations of the DOTE approach.**